Potential Encapsulating Microparticle from Degreased Dry Flour of Guava Seeds

Gustavo Rodrigues de Souza, Armanda Aparecida Júlio, Aldino Neto Venancio, Jaqueline Rodrigues Cindra de Lima Souza, Mario Ferreira Conceição Santos, Renê Chagas da Silva, Fabielle Castelan Marques, Luciano Meniniv & Tércio da Silva de Souza

Universidade Federal

ABSTRACT

Brazil is one of the world's largest producers of guava. The estimated production is approximately 552,393 tons/year. Most guava production is processed to manufacture juices, nectars, pulps, and ice creams. During the processing of guava, about 40% of the waste from the processing of guava consists of seeds, whose disposal causes environmental problems. Within this context, this work aimed to develop encapsulating material from guava seed flour and to study the kinetics, equilibrium, and thermodynamics involved in the microencapsulation process. Initially, the characterization of the guava seeds (carbohydrates, proteins, fibers, and ashes) was carried out, then the seed yield was calculated.

After the characterization, the seed yield was calculated, and these were used to prepare dry and defatted flour. This flour was characterized in terms of solubility, hygroscopicity, bed and compacted density, wettability, morphology, zero load point, and thermal analysis. The experimental parameters of the adsorption process were previously optimized.

Keywords: NA

Classification: LCC Code: TP368

Language: English

Great Britain Journals Press

LJP Copyright ID: 392943
Print ISSN: 2631-8474
Online ISSN: 2631-8482

London Journal of Engineering Research

Volume 24 | Issue 3 | Compilation 1.0

Potential Encapsulating Microparticle from Degreased Dry Flour of Guava Seeds

Gustavo Rodrigues de Souza[α], Armanda Aparecida Júlio[σ], Aldino Neto Venancio[ρ], Jaqueline Rodrigues Cindra de Lima Souza[ↀ], Mario Ferreira Conceição Santos[¥], Renê Chagas da Silva[§], Fabielle Castelan Marques[χ], Luciano Menini[ν] & Tércio da Silva de Souza[Θ]

ABSTRACT

Brazil is one of the world's largest producers of guava. The estimated production is approximately 552,393 tons/year. Most guava production is processed to manufacture juices, nectars, pulps, and ice creams. During the processing of guava, about 40% of the waste from the processing of guava consists of seeds, whose disposal causes environmental problems. Within this context, this work aimed to develop encapsulating material from guava seed flour and to study the kinetics, equilibrium, and thermodynamics involved in the microencapsulation process. Initially, the characterization of the guava seeds (carbohydrates, proteins, fibers, and ashes) was carried out, then the seed yield was calculated.

After the characterization, the seed yield was calculated, and these were used to prepare dry and defatted flour. This flour was characterized in terms of solubility, hygroscopicity, bed and compacted density, wettability, morphology, zero load point, and thermal analysis. The experimental parameters of the adsorption process were previously optimized. The adsorption capacity was evaluated in a batch system under a controlled temperature of 25 ± 2°C. From the results obtained, it is possible to infer that the dry and defatted seed flour presented the potential for the proposed purpose, with a high capacity to incorporate the methylene blue dye (~83%). The experimental results showed that the pseudo-second-order model better described the adsorption kinetics.

Finally, thermodynamic results analysis revealed a spontaneous adsorption process (ΔG°= -44.10 kJ mol^{-1}), exothermic (ΔH° = -22.47 kJ mol-1), and with ΔS° = -73 .62 J mol^{-1} K^{-1}, which shows small changes in randomness at the solute-adsorbent interface during adsorption.

Author α ¥: Universidade Federal do Espírito Santo/Departamento de Química e Física, Alto Universitário s/n, Guararema, 29500-000, Alegre-ES, Brasil.

σ ↀ ν Θ: Federal de Educação/ Ciência e Tecnologia do Espírito Santo – Campus de Alegre, BR 482, Rodovia Cachoeiro/Alegre, Km 47, Distrito de Rive - 29520-000 - Alegre-ES, Brasil.

ρ: Universidade Federal Viçosa/Departamento de Química, Avenida P. H. Rolfs,s/n, Campus Universitário, 36570-900 - Viçosa-MG, Brasil.

§: Universidade Federal Viçosa/Departamento de Física, Avenida P. H. Rolfs,s/n, Campus Universitário, 36570-900 - Viçosa-MG, Brasil.

χ: Federal de Educação, Ciências e Tecnologia do Espírito Santo Endereço: Rodovia ES-482, Cachoeiro x Alegre, Morro Grande, Cachoeiro de Itapemirim - ES, CEP: 29311-970, Brasil.

I. INTRODUCTION

The Psidium guajava L. guava is a tropical fruit characterized by a low content of carbohydrates, fats, and proteins and a high content of vitamin C (more than 100 mg/100 g of fruit) and fiber content (2.8-5.5 g/100 g of fruit) [1]. In addition to its nutritional properties, this fruit is very appetizing due to its sensory properties (taste and color) [2-3-4]. Brazil is among the largest guava producers, and guava plantations are concentrated in the Northeast and Southeast regions. Production in the country reached 552, 393 tons in 2021 [5], but the commercialization of the fruit is still national.

London Journal of Engineering Research

Although the fruit is consumed in nature, most guava production is processed to manufacture juices, nectars, pulps, ice creams, jellies and jams, ingredients for preparing yogurts, jellies, and recently, the bittersweet guatchup sauce [6-7].

During the processing stages, there is a large generation of tailings mainly composed of seeds. When improperly disposed of, these tailings can cause environmental damage and consequently become a problem of significant impact on the environment and agro-industries [8].

The waste resulting from the processing of guava is a food with great potential to compose diets for production animals [9] and food for human consumption, as it has already been used in the formulation of guava seed flour for the elaboration of bread [10-11-12]. These seeds are predominantly composed of cellulose, lignin, and lignan, which have favorable characteristics for the development of encapsulating materials, in addition to presenting biodegradability, biocompatibility, and low toxicity [13]. When used as an adsorbent or encapsulating agent, guava seed flour may have promising characteristics. However, using the microencapsulation process can solve many problems, such as increasing the stability, bioavailability, and efficiency of the action of various natural products [14].

Most encapsulating materials are polymers of plant origin due to their biodegradability, biocompatibility, and low toxicity properties [13]. These polymers can be prepared from abundant and cheap agro-industrial waste, such as seeds, peels, and fruit pomace [8]. However, the literature lacks information on this agricultural waste, from the processing of guava to preparing wall material to be used in encapsulating systems, making it possible to carry out studies to identify the potential of dry flour and defatted guava seed.

Thereby the potential of developing an innovative and technological product from low-cost and abundant agricultural waste, the present study aims to prepare to encapsulate material from the dry and defatted flour of guava seeds from agro-industrial waste.

II. EXPERIMENTAL

2.1 Guava Material

The guava waste was acquired at the fruit pulp production unit (PapaFruta®), located in the municipality of Mimoso do Sul, in the southern region of Espírito Santo, and was immediately transported in a thermal box to the Ifes Applied Chemical Laboratory - Campus Alegre. The guava seeds were separated from the residue by mechanical friction via wet and subsequently dehydrated. Their yield and proximate characterization were determined (moisture, mineral content, carbohydrates, proteins, lipids, and fibers). The material was washed with running water and subjected to sun drying for 8 hours; then, they were separated from the rest of the residue and placed in a forced air circulation oven at 55°C for 48 hours.

2.2 Preparation of Dry and Degreased Guava Seed Flour (FSDSG)

The guava seeds were ground in a Willey Marconi® knife mill, MAO 48, with a sieve of 2.0 mm opening and subsequently subjected to granulometric selection in a stainless-steel sieve at 80 Mesh. The flour produced was subjected to lipid extraction in a Soxhlet system (DiogoLab) for 6 hours, using hexane as a solvent. FSDSG was suspended in aqueous HCl solution at a concentration of 0.1 mol L^{-1}, using a 5:1 ratio, and kept under stirring at 1000 Rpm for 3 hours at 25 ± 1°C. Then the material was subjected to quantitative filtration for 24 hours and dried in an oven at 105°C for 1 hour.

2.3 Yield and Properties of FSDSG

FSDSG yield was determined by mass difference, and solubility was calculated according to the method described by Cano-Chauca et al. (2005). Wettability was determined according to the method described by Fuchs et al. (2006). Hygroscopicity was estimated according to the methodology of Cai and Corke (2000). Bed density was conducted following the methods proposed by Jinapong., Suphantharika., Jamnong (2008), and Goula and Adamopoulos (2012) with adaptations. Moisture, ash, protein, lipid, and

fiber contents were determined by standard methodologies proposed by the ASSOCIATION OF OFFICIAL ANALYTICAL CHEMISTS (CUNNIFF-AOAC, 1995). The gravimetric method determined the moisture content by drying in an oven at 105°C (QUIMIS®) until constant weight and mineral matter were obtained by incinerating the material in a muffle furnace at 550°C (QUIMIS®) for five hours. Total nitrogen was determined by the Kjeldahl method and converted into crude protein by the factor 6.25 [15]. Total lipids were determined according to the Soxhlet method using petroleum ether as the solvent and crude fiber according to the Weende method [16]. The carbohydrate content was obtained by the difference [100 – (% moisture - % lipids - % protein - % fiber - % mineral matter)]. The caloric value of the seeds was estimated using the conversion factor of 4 kcal g^{-1} for protein and carbohydrate and 9 kcal g^{-1} for lipids [17]. All assays were performed in triplicate.

2.3.1 Scanning Electron Microscope (SEM)

Morphological analysis of the degreased guava seed was performed on an energy dispersive X-ray spectrometer (EDS) coupled to a scanning electron microscope (SEM) using a JEOL JSM 6010LA SEM. The material had to go through the metallization step, being coated with Au, as it is not a conductor. All images and EDS spectrum were acquired using an acceleration voltage of 20kV and 10 mm working distance. The EDS detector window was beryllium.

2.3.2 InfraRed

The spectra were obtained in the infrared region by Fourier transform coupled with the attenuated total reflectance technique (FTIR-ATR) for products derived from guava seed and were acquired in the spectral range from 400 to 4000 cm^{-1} in the Varian 660-IR equipment.

2.3.3 Structural Property

As isotermas de adsorção/dessorção de nitrogênio foram medidas em um aparelho NOVA 1200 da Quantachrome, usando o degaseificador a vácuo a 80°C por 5h. A área superficial usando o método Brunauer-Emmett-Teller (BET) foi determinada a partir de Multi Point BET. A distribuição do tamanho de poro e do volume de poro foi obtida a partir da Teoria da Densidade Funcional (DFT), que é baseada na modelagem molecular e leva em consideração a interação direta do adsorbato com a superfície adsorvente.

2.3.4 Thermogravimetric Analysis

Nitrogen adsorption/desorption isotherms were measured on a NOVA 1200 instrument from Quantachrome, using a vacuum degasser at 80°C for 5h. The surface area using the Brunauer-Emmett-Teller (BET) method was determined from MultiPoint BET. The pore size and pore volume distribution were obtained from the Density Functional Theory (DFT), which is based on molecular modeling and considers the direct interaction of the adsorbate with the adsorbent surface.

2.3.5 Ponto de Carga Zero

The measurement of pH at zero load point (pHPCZ) was performed based on the method proposed by Mall et al. (2006), which consisted of adding 100 mg of FSDSG in Erlenmeyer containing 50 mL of distilled water with the pH values adjusted between 2.0 and 11.0 through solutions of hydrochloric acid (HCl) and sodium hydroxide (NaOH). The suspensions were kept under constant agitation at 200 rpm for 24 hours at 25°C. The initial and final pH values were measured with a pH meter (MS TECNOPON, Mpa-210). The pHPCZ was measured through the first derivative (ΔpH/initial pH) of the pH behavior curve and assigned to the point where the sums of the charges tend to zero. This procedure was performed in triplicate.

2.4 Adsorption

Methylene blue cationic dye (B. Herzog, Germany) was used as the adsorbate. The previously optimized parameters were used: mass of FSDSG 0.1 g, stirring speed = 200 rpm, and pH = 7.0. Four-milliliter aliquots were taken at predefined time intervals (10, 30, 60, 90, 120, 240, 360, and 480 min) and placed in Falcon tubes, later centrifuged (HERMLE) at 6000 rpm for five minutes. The supernatant was transferred

to a quartz cuvette for reading in a UV-Vis spectrophotometer (Agilent, Cary 60 UV/Vis) at 664 nm, and then the aliquot was returned to the system. All assays were performed in triplicate. The amount of methylene blue (MB) adsorbed on the FSDSG, qe (mg g^{-1}), was calculated by Equation 1 [18-19].

$$q_e = \frac{C_0 - C_e}{w} * V \qquad (Eq.\ 1)$$

Where C_o and Ce (mg L^{-1}) are the initial and equilibrium liquid-phase concentrations of MB, respectively, V (L) is the volume of the solution, and W(g) is the mass of FSDSG used. The same procedure was followed in batch adsorption and kinetic studies, but the aqueous samples were collected at predefined time intervals. MB concentrations were similarly measured. The amount of MB adsorbed at any time, qt (mg g^{-1}), was similarly calculated by Equation 2 (Eq. 2) [18-19].

$$q_t = \frac{C_0 - C_t}{w} * V \qquad (Eq.\ 2)$$

Where C_o and Ce (mg L^{-1}) are the initial and equilibrium liquid-phase concentrations of MB, respectively, V (L) is the volume of the solution, and W (g) is the mass of FSDSG used. The same procedure was followed in batch adsorption and kinetic studies, but the aqueous samples were collected at predefined time intervals. MB concentrations were similarly measured. The amount of MB adsorbed at any time, qt (mg g^{-1}), was similarly calculated by Equation 2 [18-19].

2.5 Adsorption Isotherm and Kinetic Models

The application of adsorption isotherms is very useful in describing the interaction between the adsorbate and the adsorbent of any system. The parameters obtained from the different models provide important information about the sorption mechanisms. For example, there are various equations for analyzing experimental adsorption equilibrium data. The Langmuir and Freundlich models are the most widely used and accepted surface adsorption models for single-solute systems. On the other hand, an interesting trend in isothermal modeling is the derivation in more than one approach, thus leading to the difference in physical interpretation. In this study, the Langmuir and Freundlich isotherms [20] were applied; table 1 shows the equations and parameters of such isotherms. Kinetic models such as pseudo-first-order [21], pseudo-second -order [22], and intraparticle diffusion model [20-21]. were used to understand the adsorption dynamics concerning time for the MB-AC-3 system. The equation and parameters of these models are shown in Table 1.

Table 1: Nonlinear kinetic, isothermal and intraparticle diffusion models

Models	Names	Expression
Isotherms	Langmuir	$Q_e = \frac{q_m b C_e}{1+bC_e}$ $R_L = \frac{1}{1+b\,C_0}$
	Freundlich	$R_l = \frac{1}{1+k_a C_e}$ $q_e = K_f C_e^{\frac{1}{n_F}}$
kinetics	Pseudofirst order	$q_t = q_e[1 - e^{K_1 t}$ $h_0 = K_1 q_e$
	Pseudo Second Order	$q_t = \frac{K_2 q_e^2 t}{1+K_2 q_e t}$ $h_2 = K_2 q_e^2$

intraparticle diffusion	$K_i = \frac{Q_t}{t^{1/2}}$ $q_t = K_{id} t^{0,5} + C$

Source: BEDIN, et al., 2018., CAZETTA et al., 2011

Langmuir's constant Ka; kf = and nF = Freundlich constants; K1 and K2 = Pseudo-first-order and pseudo-second-order constants; h0 = initial adsorption; kid= intraparticle diffusion; C = intercession

Both the adsorption isotherms and the pseudo-first and pseudo-second-order kinetic models were fitted using the nonlinear fitting method, using the Origin 8.5 software. The adequate theoretical models that describe the experimental data of the system were chosen from the correlation coefficient (R^2). In addition, the experimental data were evaluated by the chi-square (χ^2) model (Eq. 3) and by the values of normalized standard deviation (Δqe) (Eq.4) [19-20].

$$X^2 = \sum_{i=1}^{n} \frac{(q_{e\,cal} - q_{e\,exp})^2}{q_{e\,cal}} \qquad (Eq.\ 3)$$

$$\Delta_{q_e}(\%) = 100\sqrt{\frac{\Sigma[(q_{e\,exp} - q_{e\,calc})q_{e\,exp}]^2}{n-1}} \qquad (Eq.\ 4)$$

Where $q_{e\ exp}$ (mg g^{-1}) is the experimental adsorption capacity, calculated q_e (mg g^{-1}) is the adsorption capacity calculated from the kinetic model and n is the number of treatments.

2.5 Thermodynamics

The effect of temperature on the adsorption of MB dye by FSDSG particles was investigated at concentrations of 60; 75, and 90 mg L^{-1} with pH = 7.0, containing 0.1 g of FSDSG, stirring speed = 200 rpm; T = 30, 50, and 70°C kept constant through the use of an incubator bath with magnetic agitation (MARCONI/MA 085/CT). The duration of each trial was eight hours. The thermodynamic parameters of Gibbs free energy change (ΔG °, kJ mol^{-1}), enthalpy change (ΔH °, J mol^{-1}), and entropy change (ΔS°, J mol^{-1} K^{-1}) were calculated from equations 5 and 6 [24-25], Ke is the dimensionless constant obtained from the qe/Ce ratio defined through Equation 5 (Eq. 5), R is the universal gas constant (8.314 J mol^{-1} K^{-1}), and T is the temperature in Kelvin.

$$lnK_e = \frac{\Delta S}{R} - \frac{\Delta H}{RT} \qquad (Eq.\ 5)$$

R is the universal constant of ideal gases, whose value is 8.314 J mol^{-1} K^{-1}, and T is the temperature in Kelvin.

The values of ΔH and ΔS can be determined experimentally. For example, the graph of ln Ke versus 1/T generates a line, and the slope is - ΔH /R, and the linear coefficient corresponds to ΔS/R. With the values of ΔH and ΔS calculated, it is possible to calculate the Gibbs free energy (ΔG) value for a given temperature through Equation 6 (Eq.6).

$$\Delta G = \Delta H - T\Delta S \qquad (Eq.\ 6)$$

III. RESULTS AND DISCUSSION

3.1 General Characteristics and Properties of FSDSG

The encapsulating material developed is of vegetable origin and was obtained from the dried and degreased guava seed. Visually, the product appeared in the form of a fine, loose powder with light cappuccino brown colors. The results regarding the proximate composition, seed yield obtained based on the raw guava waste, properties of the dry and defatted flour of guava seeds, and the yield after standardization of granulometry at 80 mesh are presented Table 2.

Table 2: Centesimal Composition of Guava Seeds and Yield, Characterization of Dry and Defatted Guava Seed Flour and Yield

Centesimal Composition of Guava Seeds and Yield	
seed yield % (m m^{-1})	48.11 ± 0.30
Fiber % (m m^{-1})	58.15 ± 1.32
carbohydrates % (m m^{-1})	18.7 ± 1.0
lipids % (m m^{-1})	10.82 ± 0.20
proteins % (m m^{-1})	8.71 ± 0.30
energy content (kcal $100g^{-1}$)	206.2 ± 5.4
FSDSG Properties and Yield	
FSDSG Yield % (m m^{-1})	34.42 ± 0.14
Solubility % (m m^{-1})	1.95 ± 0.54
Wetability (min)*	10.13 ± 0.02
hygroscopicity (g água $100g^{-1}$)	7.33 ± 1.10
bed density (g cm^{-3})	0.29 ± 0.05
compacted density (g cm^{-3})	0.46 ± 0.04

Buoyancy and submersion time in minutes

3.2 Characterization of the Encapsulating Material

3.2.1 Morphology by Analysis of Energy Dispersive X-ray Spectroscopy Coupled to SEM.

Energy dispersive X-ray spectroscopy provides information on the chemical composition of the elements in the sample. Figure 1 and Table 3 show the relative spectrum and atomic composition of the encapsulating material, respectively, obtained from guava seed, while Figure 2 shows images representing the material's morphology at different scales.

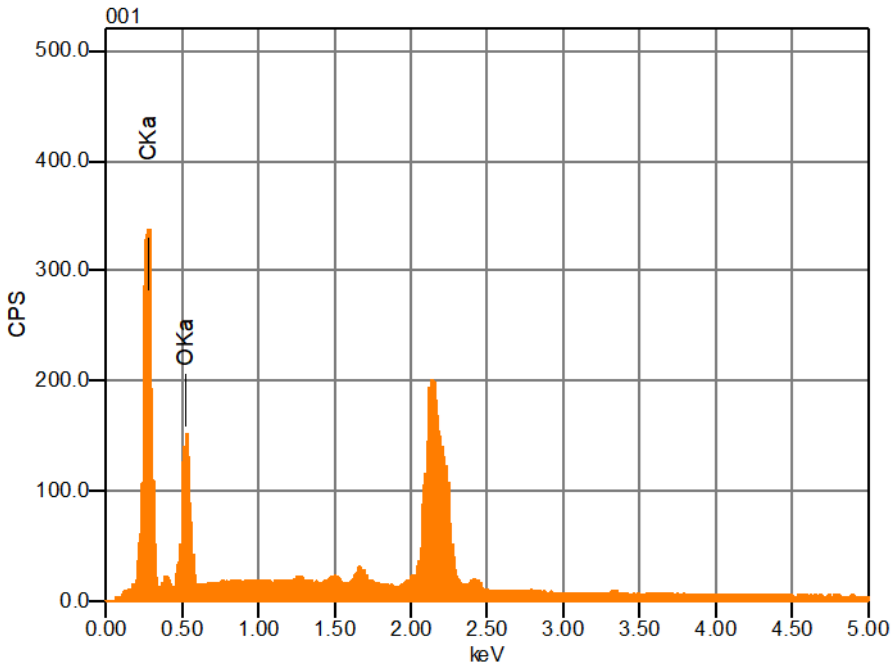

Fig. 1: EDS Spectrum of the Encapsulating Material

Table 3: Elemental Composition of the Encapsulating Material

Elements detected	Mass(%)	atom
C	60,79	67,37
O	39,21	32,63

The EDS analysis indicated that the encapsulating material obtained has only carbon (O) and oxygen (O) in its elemental composition

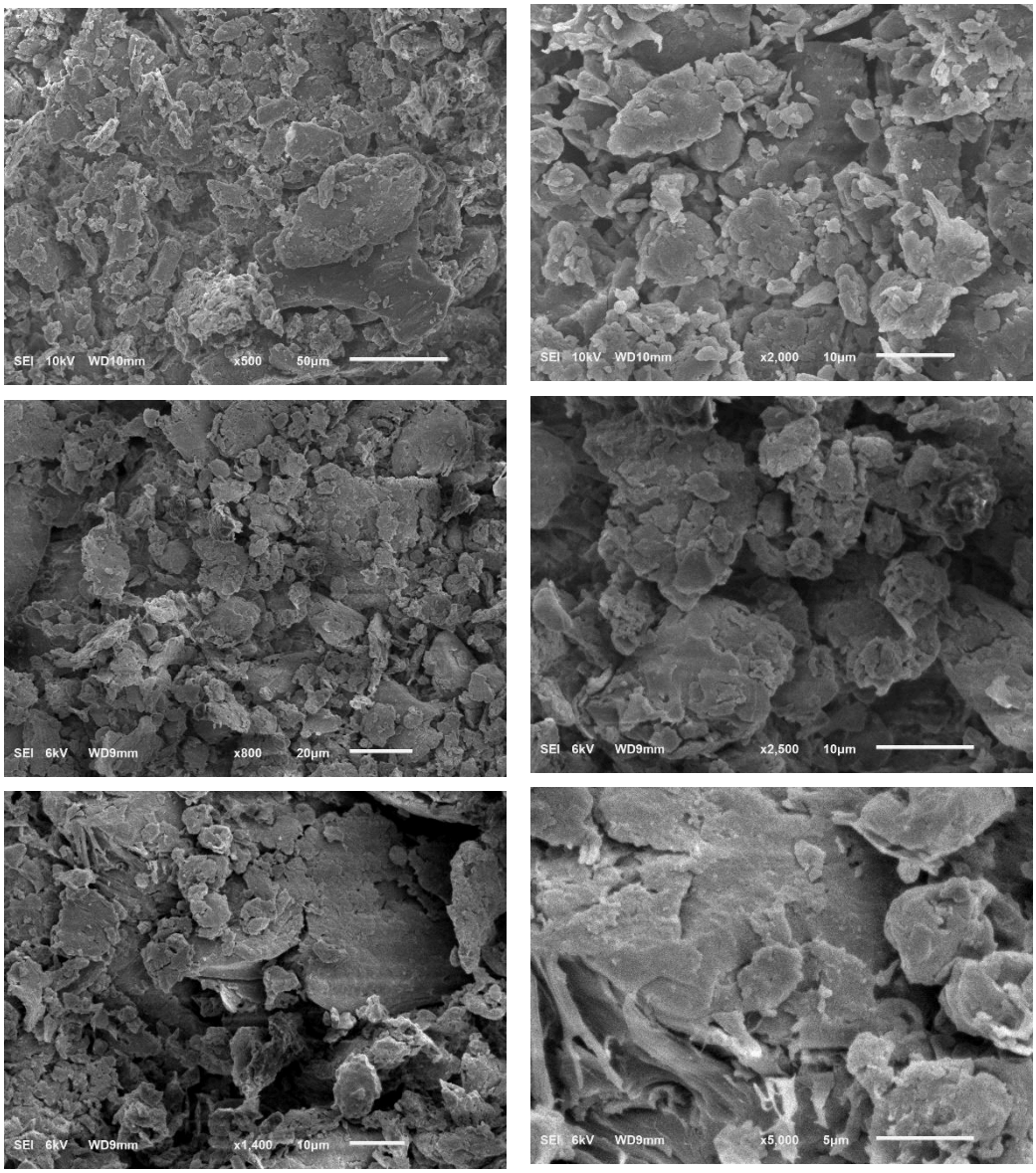

Fig. 2: Micrographs of Encapsulating Material Obtained from Guava Seeds

The SEM images at different scales show that the particles of the encapsulating material developed from degreased guava seeds have geometrically irregular surfaces. This characteristic may favor the process of microencapsulation of other materials in their structure.

3.4 Spectroscopy in the Infrared Region

Analyzing the presence of functional groups in the raw material before and after going through the lipid extraction process indicates whether there was complete removal of the lipid fraction present in the encapsulating material developed (FSDSG),

whose spectra were obtained in the infrared region and are represented in Figure 3.

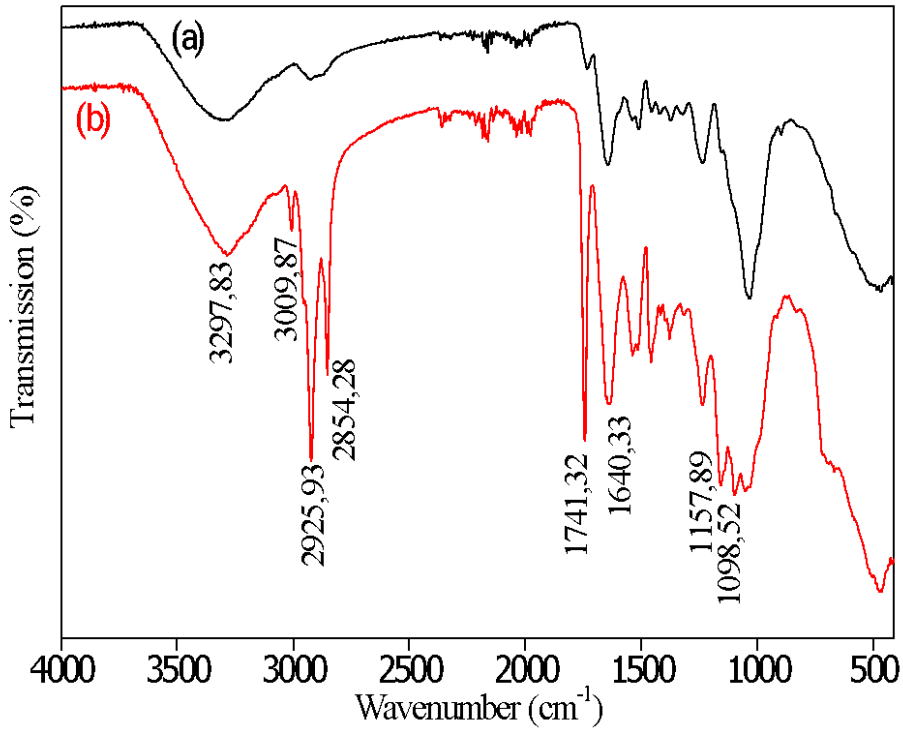

Fig. 3: Spectroscopy in the Infrared Region: (a) Dry and Defatted Guava Seed Flour (encapsulating material), (b) Dry Guava Seed Flour

It is possible to observe in Figure 3(a) that the spectrum of the encapsulating material obtained after the process of removing lipid compounds, has a spectral profile different from that of spectrum 3(b), which represents the guava seed just dry, still with lipid content gift. The spectra have bands in common, highlighting the band present at 3297.83 cm^{-1} due to the stretching of the -OH bond. At 3009.87 cm^{-1}, a band appears that can be attributed to the stretching of the N-H bond associated with amide and is consistent with the band present at 1640.33 cm^{-1}, characteristic of the amide carbonyl group, which is also common in encapsulating material developed, but it is present to a lesser extent. When analyzing spectrum 3(b), there are two bands at 2925.93 and 2854.28 cm^{-1}, which are attributed to stretching of C-H bonds with sp^3 hybridization due to symmetrical and asymmetrical vibrations of the C-H bond. The intense and narrow band present at 1741.32 cm^{-1} is typical of carbonyl stretching (C=O) as described by Pavia et al. (2010), which was consistent with the presence of fatty acid ester present in guava seed, observed in the spectrum (b), thi is the most important in the analysis performed, as it is absent in the encapsulating material, which had the acid content removed, indicating that the material had the lipid fraction successfully removed. The bands in 1157.89 and 1098.52 cm^{-1} can be attributed to the stretching of C-O bonds.

3.5 Propriedade Estrutural

Determining the textural properties of encapsulating material is of great value for the knowledge of its characteristics, as it provides essential information about the material, such as surface area, volume, and pore size, data displayed in Table 4 for the material developed. The N_2 adsorption/desorption isotherms are represented in Figure 4.

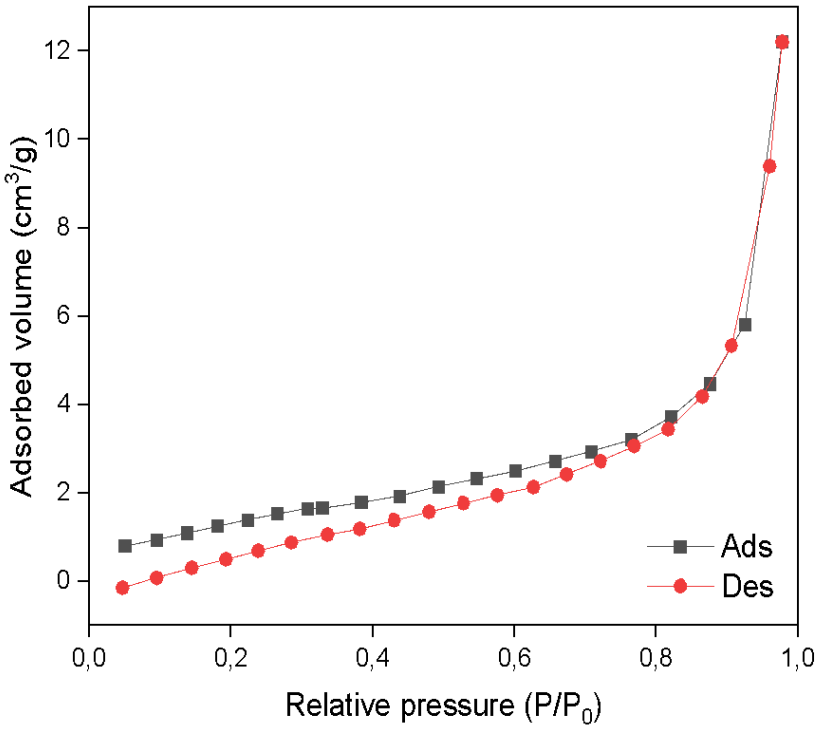

Fig. 4: Isotermas de adsorção/dessorção de N_2 da amostra FSDSG

Table 4: FSDSG sample Texture Properties Obtained from N2 Adsorption/Desorption Analysis

	Surface area (multiPoint S_{BET}) (m^2/g)	pore volume (cm^3/g)*	pore size (nm)*
FSDSG	5.401	$1.342x10^{-2}$	5.438

** DFT method*

Depending on the pore size of a material, it can be classified as macro, meso, or microporous. If the pore diameter exceeds 50 nm, it characterizes a macroporous solid, if the pore size is between 2 and 50 nm, it is characteristic of a mesoporous solid, and if the size is less than 2 nm, it is considered a microporous solid, which subdivided into solid ultra-micropores (pore diameter <0.7 nm), medium-sized micropores (0.7 nm < pore diameter <0.9 nm) and supermicropores (pore diameter >0.9 nm) [25-26]. After analyzing the results obtained in the texture analysis, it was possible to infer that the encapsulating material (FSDSG) is a mesoporous solid due to its pore size of 5.438 nm. The pore size of the material is interesting, as materials with a minimal pore size can make it difficult to encapsulate other materials in their available sites since the material to be encapsulated must be able to access the pore that the encapsulating material does. Following the classification described by the IUPAC, the N_2 adsorption/desorption isotherms have six distinct classifications. Thommes et al. (2015) describe that each isotherm characterizes a solid as a function of the pore size of the adsorption phenomenon. Type I isotherms are typical of microporous solids; types II and IV are characteristics of non-porous solids and macroporous solids, respectively. Types III and V isotherms are typical of systems where the adsorbate molecules interact more with each other than with the solid; finally, type VI

isotherms occur with the adsorption of a gas by a non-porous solid with a uniform surface, which is a rarer phenomenon. The N_2 FSDSG adsorption/desorption isotherms obtained for the material developed here are shown in Figure 4.

Due to the shape of the isotherm obtained for FSDAG, it can be inferred that the isotherm has a type IV isotherm characteristic, as Figure 4 shows a small hysteresis, which characterizes a mesoporous solid, information that corroborates the data obtained in the associated texture analysis and pore size.

3.5 Thermogravimetric Analysis

The thermogravimetric analysis was performed based on pre-defined atmospheric and temperature conditions and allowed the assessment of the material's thermal stability. This technique makes it possible to know the changes that heating can cause in the mass of substances, allowing us to establish the temperature range in which they acquire a fixed, defined, and constant chemical composition, the temperature at which they begin to decompose, and to monitor the progress of dehydration reactions (moisture loss), oxidation, combustion, and decomposition [27]. The result of the thermal analysis of the encapsulating material (FSDSG) obtained from defatted guava seeds is represented in Figure 5, where the mass loss curves (TG) and the mass loss curve derivative (DTG) are exposed.

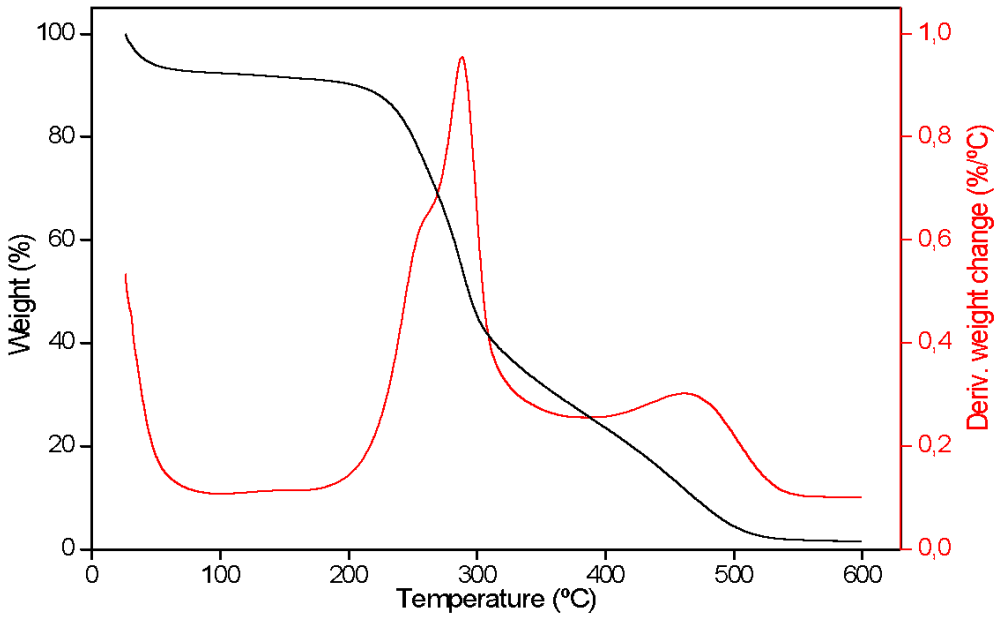

Fig. 5: Mass Loss Curve (TG) and the Derivative of Mass Loss Curve (DTG)

Looking at Figure 5, the mass loss curve of FSDSG showed a mass loss of approximately 8% during the temperature variation from 25°C to 175°C, resulting from the loss of residual water from the sample. However, the significant mass loss occurred between 225°C and 375°C. Through the DTG curve, it was possible to determine the temperature at which the maximum mass change rate (decomposition) is around 288°C, indicating that the material is thermally stable up to a temperature of 225°.

It is essential to know the thermal stability of material under development, as it makes it possible to predict its applications in several areas. For example, when referring to HTST (High-Temperature Short Time), heat treatment processes combine heat, humidity, and mechanical work, profoundly modify the raw materials and provide new formats and structures with different functional and nutritional characteristics [28]. Among these materials

industrialization processes, we can highlight the extrusion process, which has been widely used in the last decades in the food industries due to its numerous advantages such as versatility, continuous production on a large scale, and per unit area low cost. With investment, labor, and energy, the quality of products with better functional, sensory, and nutritional characteristics is a process that does not generate effluents [29].

Aiming at the possible use of FSDSG as an encapsulating material, it is possible to carry out microencapsulation tests up to a temperature close to 225°C, above this value. The material begins the process of degradation of its chemical composition.

3.6 Point of Zero Charge

The point of zero charges (pHpcz) is one of the essential characteristics of the surface of adsorbent material, as it corresponds to the pH value of the liquid surrounding the material when the sum of the positive charges is equivalent to the sum of the negative charges on the surface. The pH_{PCZ} value characterizes the acidity of the material's surface [30-31]. Thus, in an aqueous medium, the particles have a positive surface charge if the pH of the solution is lower than the pH_{PCZ} and a negative surface charge if the pH of the solution is higher than the pH_{PCZ} [32]. The results referring to the determination of the pH_{PCZ} of the FSDSG are shown in Figure 6.

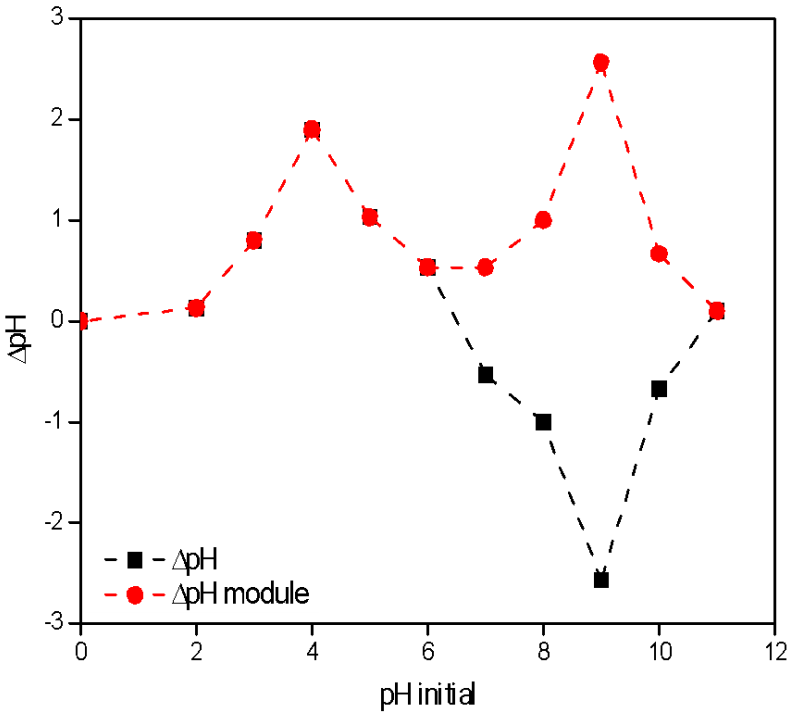

Fig. 6: Determination of pH at Zero Load point of Dry and Defatted Guava Seed Flour at 80 Mesh

To understands the adsorption mechanism, is necessary to determine the pHPCZ. The adsorption of cationic dyes is favored at pH higher than pHPCZ, while the adsorption of anionic dyes is favored at pH lower than pHPCZ [33]. Thus, according to Figure 6, the pHPCZ FSDSG is equivalent to 2.0 and 11.0. In the pH range below 2.0 and above 11.00, the surface charges of the material are predominantly negative. Adsorption, for example, essential (nonpolar) oils, may be preferable at these pH values. Above 2.0 and below 11.00, its surface predominates positive charge, favoring polar molecules' adsorption.

3.7 Adsorption Isotherm

The Langmuir isotherm was obtained through the correlation between Ce/qe as a function of Ce. The values of kL and qm were determined, respectively, from the linear and angular coefficients of the equation obtained by the linear regression of the line, allowed assessing whether the adsorption process is favorable (Table 5).

Table 5: Langmuir Isotherm Parameter Values for MB Adsorption by FSDSG Microparticles

Parameter	Value
Q_{max} (mg g^{-1})	57,95
K_L (L mg^{-1})	8,9645
R_L	0,0037 – 0,0012
R^2 adjusted	0,9613

Analyzing the Langmuir isotherm data, it is evident that the adsorption process fits this model well since the adjusted R^2 value is 0.9613, and the RL values, whose range is between zero and one, indicate that adsorption is favorable [34]. The value of the maximum adsorption capacity, qmax (mg g^{-1}), is essential to identify the adsorbent with the highest adsorption capacity [35]. The value of qmax depends on several factors, such as the adsorbent's characteristics and mass and the adsorbate's volume and concentration. The FSDSG microparticles used in this study showed a promising MB incorporation capacity, showing that they are suitable for incorporating active principles.

The Freundlich isotherm was obtained by correlating ln qe as a function of ln Ce. The kf 1/n values were determined by the linear and angular coefficients of the equation obtained by the linear regression of the line. These parameters and the adjusted R^2 value are represented in Table 6.

Table 6: Values of Freundlich Isotherm Parameters for Adsorption of MB by FSDSG Microparticles

Parameter	Value
K_f (L mg^{-1})	1,0155
1/n	0,5679
n	1,7609
R^2 adjusted	1,0000

Analyzing the data found for this model, it is evident that it has an adjusted R^2 value above 0.9999. Thus, the experimental data fit well to this model, which considers the adsorbent constituted of multiple layers and is applicable for reversible adsorption on heterogeneous surfaces, with available sites with different adsorption energies [36].

The value of 1/n less than 1.0 indicates that the adsorption applies to the range of MB concentrations evaluated in this study [37] and reveals that the adsorption occurs by heterogeneous means, with the high-energy sites being occupied first. Then adsorption occurs at lower-energy sites [38]. The value of n greater than 1.0 shows that the process of adsorption of MB by the FSDSG microparticles was favorable.

3.8 Adsorption Studies

The results for the pseudo-first-order kinetic model were obtained through the linearized Lagergren equation, through the construction of a graph of ln (qe - qt) as a function of time for each value of the initial concentration of MB. The values corresponding to qe for the linearized Lagergren equation were those obtained experimentally (qe exp). The parameters calculated qe (qe calc) and k1 were determined from the linear and angular coefficients of the equations formed by the regression of ln (qe - qt) as a function of time. These parameters and the values of the correlation coefficient (R^2) adjusted normalized standard deviation (Δqe), and the chi-square model (χ^2) are presented in Table 7.

Table 7: Kinetic Parameters for the Pseudo-First-Order model, Chi-square model (χ2), and normalized standard deviation ($\Delta_q e$) of different initial concentrations of MB

	Initial Concentrations (mg L^{-1})				
	30	45	60	75	90
$q_{e\ exp}$ (mg g^{-1})	13.84	19.80	26.02	32.12	37.48
$q_{e\ calc}$ (mg g^{-1})	0.65	16.75	15.7	21.97	32.49
K (min^{-1})	-0.0001	-0.0039	-0.0019	-0.0024	-0.0042
R^2 adjusted	0.0006	0.5006	0.1203	0.2506	0.4590
Δq_e	47.6567	7.6908	20.0860	15.8002	6.6594
X^2	268.1992	0.5536	7.0180	4.6900	0.7670

After analyzing the R^2 values, it is evident that the adsorption process does not present a good fit for the pseudo-first-order kinetic model. Further more, there is a discrepancy between the experimental and calculated qe values. These data suggest that the process of MB adsorption by FSDSG microparticles does not follow this kinetic model.

The k_1 parameter plays a time scaling factor. The higher the value of k_1, the shorter the time taken for the adsorption system to reach equilibrium. Relatively high values of k1 indicate shorter times for the system to reach equilibrium. However, some studies report that the value of k1 may be linked to the dependence or independence of operating conditions [35].

A low correlation coefficient was found with the application of this model. This parameter cannot be used in this work to evaluate the speed with which the system reaches equilibrium. Pseudo-first order kinetics is controlled by diffusion through the boundary layer around the adsorbent solid [35]. Therefore, it is possible to state that diffusion is not the determining step of the process in question since this model did not present a good fit for the experimental data.

In the pseudo-second-order kinetic model for the adsorption of MB by the FSDSG microparticles, the values of q_e exp, q_e calc, and k_2 were obtained using the linearized equation and building a graph t/qt as a function of time for each value of the initial concentration of MB, these parameters and the adjusted R^2 values are shown in Table 8.

Table 8: Kinetic parameters for the pseudo-second order model, chi-square model (χ2) and normalized standard deviation (Δqe) of different initial concentrations of MB

	Initial Concentrations (mg L^{-1})				
	30	45	60	75	90
$q_{e\ exp}$ (mg g^{-1})	13.84	19.80	26.02	32.12	37.48
$q_{e\ calc}$ (mg g^{-1})	14.30	19.72	25.75	31.76	37.21
K_2 (min^{-1})	0.0750	0.0505	0.0382	0.0309	0.0266
R^2 adjusted	0.9982	0.9999	0.9999	0.9999	0.9999
Δq_e	2.3866	0.0606	0.2567	0.2875	0.1807
X^2	0.1080	0.0001	0.0028	0.0043	0.0020

Through Table 8, was possible to observe the data obtained through the adjustment performed by the kinetic model of pseudo-second-order adsorption. This model's correlation coefficient (R^2) was more significant than 0.99 at different concentrations. The applicability of the pseudo-second-order kinetics model was confirmed by the low values of normalized standard deviation (Δqe). Was also possible to observe that the calculated qe values obtained through the adjustment are very close to the experimental q_e.

It is evidenced that K_2 values decrease with increasing concentration. These low values show that the adsorption process is slow, and equilibrium was not reached quickly. The oscillations of these values are linked to the operational conditions and the initial concentration of solute [35].

Kinetic studies are essential tools for understanding the interaction dynamics between the adsorbent and the adsorbate. These provide information that can help model and design adsorption processes. For example, the adsorption kinetics data for MB dye were analyzed using the pseudo-second-order kinetic model shown in Figure 7.

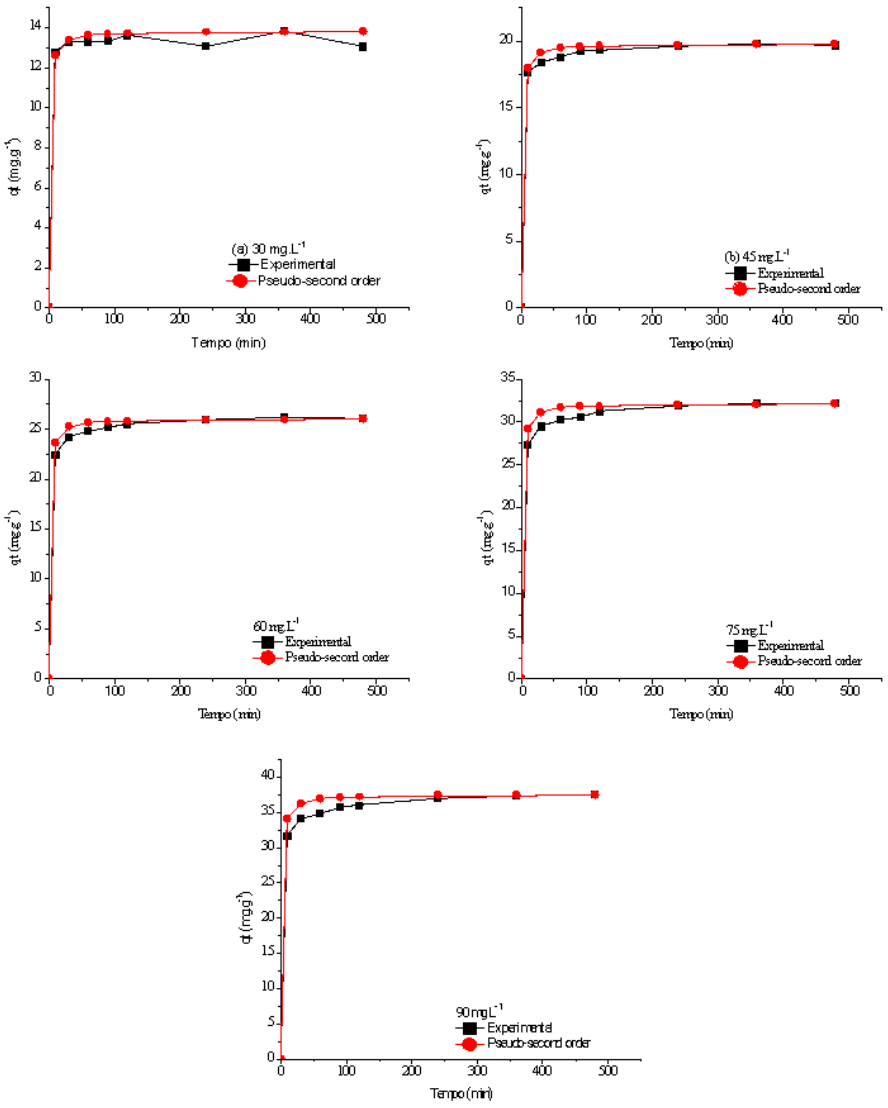

Fig. 7: Non-linear fit of the pseudo-second order kinetic study for different MB concentrations. MB concentrations of 30 (a), 45 (b), 60 (c), 75 (d) and 90 (e) mg L^{-1}

According to Figure 7, the MB dye adsorption system by the FSDSG microparticles reached equilibrium during the first 60 min of the test, demonstrating that the interactions were favorable between the adsorbent and the adsorbate.

The model based on the theory described by Weber and Morris (1963) was applied to the adsorption system to identify the intraparticle diffusion mechanism. The value found through the slope of the line corresponds to the intraparticle diffusion constant (k_{di}). In contrast, the approximate value of the boundary layer thickness (C_i) is obtained at the intercept of the line. The intraparticle diffusion model can generally occur through the following steps: external diffusion, surface diffusion, and pore diffusion [39].

Table 9 shows the values of kdi, C_i, and correlation coefficient (R^2) obtained for the different concentrations. The (R^2) values are smaller than predicted by the pseudo-second-order model, so the experimental q_e value does not agree well with the intraparticle diffusion model.

Table 9: Intraparticle Diffusion Model Constants and Correlation Coefficients for Adsorption

	intraparticle Diffusion		
C_o (mg L^{-1})	K_{di} (mg g^{-1} $min^{-1/2}$)	C_i (mg g^{-1})	R^2
30	0.0404	12.57	0.1191
45	0.0997	17.90	0.7930
60	0.1637	23.10	0.7506
75	0.2167	28.33	0.6929
90	0.2715	32.33	0.8301

The values related to the five different initial concentrations showed two stages of linearity. The first stage was completed in the first 60 min, known as instantaneous adsorption. The second region is the gradual adsorption stage, where intraparticle diffusion is the rate-limiting. The linear behavior did not pass through the origin or close to saturation, which indicates that intraparticle diffusion is not the step that determines the rate of adsorption, so other interaction mechanisms must act simultaneously to control the adsorption process [40-41-42-43].

3.9 Thermodynamic

The thermodynamic study is based on the determination of quantities, enthalpy variation (ΔH°), entropy variation (ΔS°), and variation of Gibbs free energy (ΔG°). By estimating these thermodynamic parameters, it is possible to determine whether the process is spontaneous, exothermic, or endothermic and whether the adsorbent material has an affinity for the adsorbate. In addition, these parameters can provide information regarding the heterogeneity of the adsorbent surface and whether the process involves physical or chemical adsorption [44].

Table 10 shows the values of the Gibbs free energy variation (ΔG°), kc, and adjusted correlation coefficient (R^2), obtained for the adsorption of MB dye by FSDSG microparticles at 60, 75, and 90 mg L^{-1}. From the thermodynamic data, was possible to verify that ΔG° varies from -28.80 to -64.86 kJ mol^{-1}, having significant oscillations during the adsorption process.

Table 10: Values of Gibbs free energy variation (ΔG°), kc and adjusted correlation coefficient (R2) for the adsorption of methylene blue by FSDSG microparticles

Concentration (mg L^{-1})	kc	ΔG° (kJ mol^{-1})	R^2
60	3.52	-44.10	0.9999
75	2.10	-64.86	0.8619
90	1.62	-28.80	0.9295

London Journal of Engineering Research

With the initial concentration of MB of 60 mg L^{-1}, obtaining the highest correlation coefficient (R^2) adjusted for the adsorption was possible. Therefore, this condition was selected to monitor the adsorption process and to determine the values of ΔH, and ΔS. Table 11 shows the values of the Gibbs free energy change ((ΔG° kJ mol^{-1}), kc, enthalpy change (ΔH, kJ mol^{-1}) and entropy change (ΔS, J mol^{-1}) K^{-1}) for the adsorption of MB by the FSDSG microparticles at an initial concentration of 60 mg L^{-1}.

Table 11: Values of (ΔG° kJ mol^{-1}), kc, (ΔH°, kJ mol^{-1}) and (ΔS°, J mol-1 K^{-1}) for the adsorption of AM dye by FSDSG microparticles on initial concentration of 60 mg L-1

T (K)	k_c	ΔG° (KJ mol^{-1})	ΔH° (KJ mol^{-1})	ΔS° (J $mol^{-1}K^{-1}$)
303.15	3.5	-22.34		
323.15	2.4	-46.26	-22.47	-73.62
343.15	1.8	-47.73		

The results concerning the thermodynamics of the adsorption process revealed that it is spontaneous (ΔG° = -46.26 kJ mol^{-1}) and exothermic (ΔH° = -22.47 kJ mol^{-1}). The negative value of ΔS° (-73.62 J mol^{-1} K^{-1}) suggests that the dye molecules are stable on the surface of the adsorbent and that there is a decrease in randomness at the solid-solute interface during adsorption. In addition, the value confirms the affinity of the adsorbent material for the dye.

With increasing temperature, a reduction in adsorption at equilibrium occurs, causing a decrease in kc values and an increase in ΔG°, indicating a reduction in spontaneity. The increase in the value of ΔG° being proportional to the increase in temperature indicates that the lower the temperature, the easier the adsorption [45]. This decrease in adsorption capacity can be explained by the increase in temperature, which possibly causes an increase in MB solubility, which makes its adsorption difficult since the dye will have more affinity with the solvent than with the adsorbent.

Ahmad and Kumar (2010b) reported that the enthalpy change due to chemisorption has values between 84 - 420 KJ mol^{-1}. Thus, enthalpy values below 84 KJ mol^{-1} indicate that the nature of adsorption is physical, involving weak attractive forces [46]. Entropy is entirely linked to disorganization at the adsorbent/adsorbate interface. Positive values of ΔS are interpreted as an increase in disorganization at the adsorbent material interface [40].

IV. CONCLUSION

This work made it possible to prepare good quality encapsulating material with guava seeds, as demonstrated by the characterization tests. In addition, a good yield of flour mass was obtained through cheap and abundant agro-industrial waste. The results showed that the material has promising physical and chemical characteristics as an encapsulating material for the methylene blue dye.

The adsorption of methylene blue by microparticles of dry and defatted guava seed flour is best explained by the pseudo-second-order model, indicating that the adsorption is controlled by sharing or transferring electrons between the adsorbent and adsorbate molecules. Regarding the adsorption equilibrium, the experimental results adjusted all tested isothermal models.

The results referring to the thermodynamics of the adsorption process revealed that it was spontaneous and exothermic. The negative value of ΔS suggests that the dye molecules are stable on the surface of the adsorbent and that there is a decrease in randomness at the solid-solute interface during adsorption. In addition, the value confirms the affinity of the adsorbent material for the dye.

REFERENCE

1. PÉREZ GUTIÉRREZ, R. M., MITCHELL, S., & VARGAS SOLIS, R. Psidium guajava: a review of its traditional uses, phytochemistry and pharmacology. Journal of Ethnopharmacology, 117(1), 1–27, 2008. https://doi.org/10.1016/j.jep.2008.01.025.
2. STEINHAUS, M., SINUCO, D., POLSTER, C., OSORIO, C., & SCHIEBERLE, P. (2008). Characterization of the aroma-active compounds in pink guava (Psidium guajava L.) by application of the aroma extract dilution analysis. Journal of Agricultural and Food Chemistry, 56(11), 4120–4127, 2008. https://doi.org/10.1021/jf8005245.
3. MERCADANTE, A. Z., STECK, A., & PFANDER, H. (1999). Carotenoids from guava (Psidium guajava L.): Isolation and structure elucidation. Journal of Agricultural and Food Chemistry, 47(1), 145–151. https://doi.org/10.1021/jf980405r.
4. GONZÁLEZ, I. A., OSORIO, C., MELÉNDEZ-MARTÍNEZ, A. J., GONZÁLEZ-MIRET, M. L., & HEREDIA, F. J. Application of tristiumuls colorimetry to evaluate color changes during the ripening of Colombian guava (Psidium guajava L.) varieties with different carotenoid pattern. International Journal of Food Sciences and Nutrition, 46(4), 840–848, 2011. https://doi.org/10.1111/j.1365-2621.2011.02569.x.
5. IBGE – Instituto Brasileiro de Geografia e Estatística – SIDRA - Produção Agrícola Municipal 2021 - Tabela 5457 - Área plantada ou destinada à colheita, área colhida, quantidade produzida, rendimento médio e valor da produção das lavouras permanentes (notas). Disponível em https://cidades.ibge.gov.br/brasil/pesquisa/15/0, acesso em 17/out. 2022.
6. EMBRAPA - Coleção Plantar. 66 (2010). A cultura da goiaba [editores técnicos: Flávia Rabelo Barbosa e Mirtes Freitas Lima] – 2ª edição revista e ampliada – Brasília, DF: Embrapa Informação Tecnológica, 2010. 180p. Disponível em: https://ainfo.cnptia.embrapa.r/digital/bitstream/item/128279/1/PLANTAR-Goiaba-ed02-2010.pdf
7. OSORIO, C.; FORERO, D.P.; CARRIAZO, J. G. Characterisation and performance assessment of guava (Psidium guajava L.) microencapsulates obtained by spray-drying. Food Research International, v. 44, n. 5, p. 1174-1181, 2011. https://doi.org/10.1016/j.foodres.2010.09.007.
8. SOUZA, G. R., NASCIMENTO M., E., OLIVEIRA S., P., MERSON, A. A., LIMA S., J. R. C., MARQUES, F. C., SOUZA, T. D. S. Desenvolvimento de material encapsulante a partir da farinha seca e desengordurada de semente de goiaba. Brazilian Journal of Development, v. 6, n. 12, p. 98027-98037, 2020. https://doi.org/10.34117/bjdv6n12-337
   CANO-CHAUCA, M et al. Effect of the carriers on the microstructure of mango powder obtained by spray drying and its functional characterization. Innovative Food Science & Emerging Technologies, v. 6, n. 4, p. 420-428, nov./dez, 2005. https://doi.org/10.1016/j.ifset.2005.05.003
   FUCHS, M. et al. Encapsulation of oil in powder using spray drying and fluidised bed agglomeration. Journal of Food Engineering, v. 75, n. 1, p. 27–35, jun./jul, 2006. doi: https://doi.org/10.1016/j.jfoodeng.2005.03.047
   CAI, Y. Z.; CORKE, H. Production and Properties of Spray-dried Amaranthus Betacyanin Pigments. Journal of food science, Chicago, v. 65, n. 3600, p. 1248–1252, jun./jul. 2006. https://doi.org/10.1111/j.1365-2621.2000.tb10273.x.
   JINAPONG, N.; SUPHANTHARIKA, M.; JAMNONG, P. Production of instant soymilk powders by ultrafiltration, spray drying and fluidized bed agglomeration. Journal of Food Engineering, Essex, v. 84, n. 2, p. 194–205, dez./jan. 2008. https://doi.org/10.1016/j.jfoodeng.2007.04.032.
   GOULA, A. M.; ADAMOPOULOS, K. G. A method for pomegranate seed application in food industries: Seed oil encapsulation. Food and Bioproducts Processing, Rugby, v. 90, n. 4, p. 639-652, set./out, 2012. https://doi.org/10.1016/j.fbp.2012.06.001.
9. SILVA, E. P. D., SILVA, D. A. T. D., RABELLO, C. B. V., LIMA, R. B., LIMA, M. B.,

& LUDKE, J. V. Composição físico-química e valores energéticos dos resíduos de goiaba e tomate para frangos de corte de crescimento lento. Revista Brasileira de Zootecnia, v. 38, n. 6, p. 1051-1058, 2009. Disponível em: https://www.scielo.br/j/rbz/a/vK3tG7XYc9fpHVZc6zd5qNc/?format=pdf&lang=pt.

10. SILVEIRA, MÁRCIA LILIANE RIPPEL et al SILVEIRA, M. L. R., DOS SANTOS, C. O., PENNA, N. G., SAUTTER, C. K., DA ROSA, C. S., & BERTAGNOLLI, S. M. M. Aproveitamento tecnológico das sementes de goiaba (Psidium guajava L.) como farinha na elaboração de biscoitos. Boletim do Centro de Pesquisa de Processamento de Alimentos, v. 34, n. 2, 2017. http://dx.doi.org/10.5380/cep.v34i2.53178.
11. SOARES, D. J., DIOGENES, A., MOURA NETO, L. G., COSTA, Z. R. T., ALVES, V. R., SANTOS, M., & MORAIS, B. Utilização de farinha de resíduos de goiaba na elaboração de pães. Revista CIENTEC, v. 9, n. 1, p. 97-103, 2017. Disponível em: http://revistas.ifpe.edu.br/index.php/cientec/article/view/39/32.
12. THOMAZ, A. U., SOUSA, E. C., LIMA, A., LIMA, R. M. T., FREITAS, P. A. P., SOUZA, M. A. M., & CARIOCA, J. O. B. Elaboração e aceitabilidade de produtos de panificação enriquecidos com semente de goiaba (Psidium guajava L.) em pó. HOLOS, v. 5, p. 199-210, 2014. https://doi.org/10.15628/holos.2014.1895.
13. LUO, Ye WANH, Q. Zein based micro and nano-particles for drug and nutrinet delivery: A review. Journal of Applied Polymer Science. v. 131, n. 16, p. 1-12, 2014. https://doi.org/10.1002/app.40696.
14. SILVA, P. T. D., FRIES, L. L. M., MENEZES, C. R. D., HOLKEM, A. T., SCHWAN, C. L., WIGMANN, É. F., & SILVA, C. D. B. D. Microencapsulation: concepts, mechanisms, methods and some applications in food technology. Ciência Rural, v. 44, p. 1304-1311, 2014. http://dx.doi.org/10.1590/0103-8478cr20130971.
15. GALVANI, F; GAERTNER, E. Adequação da metodologia Kjeldahl para determinação de nitrogênio total e proteína bruta. Embrapa Pantanal-Circular Técnica (INFOTECA-E), 2006. Disponível em: http://www.infoteca.cnptia.embrapa.br/infoteca/handle/doc/812198.
16. WILLIAMS, R. D. e OLMSTED, W. H. A biochemical method for determining indisgetible residue (crude fiber) in feces: lignin, cellulose, and non-water-soluble hemicelluloses. Journal of Biological Chemistry, v. 108, n. 3, p. 653-666, abr/mar, 1935. Disponível em: https://www.cabdirect.org/cabdirect/abstract/19351400053.
17. MERRILL, A. L. e BERNICE, K. W. (1973). Energy Value of Foods: Basis and Derivation. Agriculture Handbook. Washington, DC, ARS United States Departament of Agriculture. Disponível em: https://www.ars.usda.gov/ARSUserFiles/80400525/Data/Classics/ah74.pdf.

    MALL, I.D., SRIVASTAVA, V.C., KUMAR, G.V.A., AND MISHRA, I.M. Characterization and utilization of mesoporous fertilizer plant waste carbon for adsorptive removal of dyes from aqueous solution. Colloids and Surfaces A: Physicochemical and Engineering Aspects, cidade, v. 278, n. 1-3, p. 175-187, 2006. doi: 10.1016/j.colsurfa.2005.12.017. https://doi.org/10.1016/j.colsurfa.2005.12.017.
18. BEDIN, K. C., SOUZA. I. P. A. F., CAZETA, A. L., SPESSATO L. RONIX A. ALMEIDA. V. C.CO2-spherical activated carbon as a new adsorbent for Methylene Blue removal: Kinetic, equilibrium and thermodynamic studies. Journal of Molecular Liquids, v. 269, p. 132-139, 2018. https://doi.org/10.1016/j.molliq.2018.08.020
19. CAZETTA, A. L., VARGAS, A. M., NOGAMI, E. M., KUNITA, M. H., GUILHERME, M. R., MARTINS, A. C., ALMEIDA, V. C. NaOH-activated carbon of high surface area produced from coconut shell: Kinetics and equilibrium studies from the methylene blue adsorption. Chemical Engineering Journal, v. 174, n. 1, p. 117-125, 2011. https://doi.org/10.1016/j.cej.2011.08.058.
20. ROYER, B., CARDOSO, N. F., LIMA, E. C., VAGHETTI, J. C., SIMON, N. M., CALVETE, T., & VESES, R. C. Applications of Brazilian pine-fruit shell in natural and carbonized forms as adsorbents to removal of methylene

blue from aqueous solutions—Kinetic and equilibrium study. Journal of hazardous materials, v. 164, n. 2-3, p. 1213-1222, 2009. https://doi.org/10.1016/j.jhazmat.2008.09.028.

21. MALASH, G. F.; EL-KHAIARY, M. I. Piecewise linear regression: A statistical method for the analysis of experimental adsorption data by the intraparticle-diffusion models. Chemical Engineering Journal, v. 163, n. 3, p. 256-263, 2010. https://doi.org/10.1016/j.cej.2010.07.059.
    MALASH, G.F.; EL-KHAIARY, M. I. Methylene blue adsorption by the waste of Abu-Tartour phosphate rock. Journal of colloid and interface science, v. 348, n. 2, p. 537-545, 2010. https://doi.org/10.1016/j.jcis.2010.05.005.
22. R. HAN, J. ZHANG, P. HAN, Y. WANG, Z. ZHAO, M. TANG. Study of equilibrium, kinetic and thermodynamic parameters about methylene blue adsorption onto natural zeolite. Chemical Engineering Journal, v. 145, n. 3, p. 496-504, 2009. https://doi.org/10.1016/j.cej.2008.05.003.
23. CARDOSO, N.F., PINTO, R.B., LIMA, E.C., CALVETE, T., AMAVISCA, C.V., ROYER, B., CUNHA, M.L., FERNANDES, T.H.M., AND PINTO, I.S., Removal of remazol black B textile dye from aqueous solution by adsorption. Desalination, v. 269, n.1-3, p. 92-103, 2011. Disponível em: https://www.academia.edu/12233601/Removal_of_remazol_black_B_textile_dye_from_aqueous_solution_by_adsorption.
24. GAO, Q., ZHU, H., LUO, W.-J., WANG, S., AND ZHOU, C.-G., Preparation, characterization, and adsorption evaluation of chitosan-functionalized mesoporous composites. Microporous and Mesoporous Materials, v. 193, p. 15-26, jun./jul, 2014. doi: 10.1016/j.micromeso.2014.02.025. https://doi.org/10.1016/j.micromeso.2014.02.025.
    PAVIA et al. Introduction of Spectrocopy. 4ª edição. Cegage Learning, 2010.
25. BARDESTANI, R.; PATIENCE, G. S.; KALIAGUINE, S.. Experimental methods in chemical engineering: specific surface area and pore size distribution measurements - BET, BJH, and DFT. The Canadian Journal of Chemical Engineering, v. 97, n. 11, p. 2781-2791, 2019. https://doi.org/10.1002/cjce.23632.
26. BAE, Y-S.; YAZAYDIN, A. Ö.; SNURR, R. Q. Evaluation of the BET method for determining surface areas of MOFs and zeolites that contain ultra-micropores. Langmuir, v. 26, n. 8, p. 5475-5483, 2010. https://doi.org/10.1021/la100449z.
    THOMMES M.; KANEKO K.; NEIMARK A. V.; OLIVIER J. P.; RODRIGUEZREINOSO F.; ROUQUEROL J.; SING K. S. W. Physisorption of gases, with special reference to the evaluation of surfasse area and pore size distribution (IUPAC Technical Report). Pure and Applied Chemistry. V. 87, p. 1051 - 1070, 2015. https://doi.org/10.1515/pac-2014-1117.
27. CANEVAROLO JR, Sebastião V. et al. Técnicas de caracterização de polímeros. Artliber, São Paulo, v. 430, n. 2004, 2004. Disponível em: https://www.artliber.com.br/amostra/tecnicas_de_caracterizacao_de_polimeros.pdf
28. ZHAO, L. G.; WARRIOR, N. A.; LONG, A. C. A thermo-viscoelastic analysis of process-induced residual stress in fibre-reinforced polymer–matrix composites. Materials Science and Engineering: A, v. 452, p. 483-498, 2007. https://doi.org/10.1016/j.msea.2006.10.060.
29. GUERREIRO, L. Dossiê técnico: produtos extrusados para consumo humano, animal e industrial. Rio de Janeiro: REDETEC, 2007. Disponível em: http://www.respostatecnica.org.br/dossie-tecnico/downloadsDT/MTcy.
30. MAITY, J. AND RAY, S.K. Enhanced adsorption of methyl violet and congo red by using semi and full IPN of polymethacrylic acid and chitosan. Carbohydrate Polymers, v. 104, n. s/n, p. 8-16, mar./abr, 2014. https://doi.org/10.1016/j.carbpol.2013.12.086.
31. GEZICI, O., KÜÇÜKOSMANOĞLU, M., AYAR, A. The adsorption behavior of crystal violet in functionalized sporopollenin-mediated column arrangements. Journal of Colloid and Interface Science, v. 304, n. 2, p. 307-316, 2006. doi: 10.1016/j.jcis.2006.09.0

48. disponível em: https://ur.booksc.eu/book/3654027/7b8f64.
32. KHAN, T.A., CHAUDHRY, S.A., AND ALI, I. Equilibrium uptake, isotherm and kinetic studies of Cd(II) adsorption onto iron oxide activated red mud from aqueous solution. Journal of Molecular Liquids, v. 202, p. 165-175, 2015. https://doi.org/10.1016/j.molliq.2014.12.021.
33. MALL, I.D., SRIVASTAVA, V.C., KUMAR, G.V.A., AND MISHRA, I.M. Characterization and utilization of mesoporous fertilizer plant waste carbon for adsorptive removal of dyes from aqueous solution. Colloids and Surfaces A: Physicochemical and Engineering Aspects, cidade, v. 278, n. 1-3, p. 175-187, 2006. doi: 10.1016/j.colsurfa.2005.12.017. https://doi.org/10.1016/j.colsurfa.2005.12.017.
34. TANHAEI, B., AYATI, A., LAHTINEN, M., AND SILLANPÄÄ, M., Preparation and characterization of a novel chitosan/Al2O3/magnetite nanoparticles composite adsorbent for kinetic, thermodynamic and isotherm studies of Methyl Orange adsorption. Chemical Engineering Journal, v. 259, p. 1-10, 2015. https://doi.org/10.1016/j.cej.2014.07.109.
35. PLAZINSKI, W., RUDZINSKI, W., AND PLAZINSKA, A. Theoretical models of sorption kinetics including a surface reaction mechanism: A review. Advances in Colloid and Interface Science, v. 152, n. 1-2, p. 2-13, nov./dez, 2009. https://doi.org/10.1016/j.cis.2009.07.009.
36. DAHRI, M.K., KOOH, M.R.R., LIM, L.B.L., Water remediation using low cost adsorbent walnut shell for removal of malachite green: Equilibrium, kinetics, thermodynamic and regeneration studies. Journal of Environmental Chemical Engineering, v. 2, n. 3, p. 1434-1444, 2014. https://doi.org/10.1016/j.jece.2014.07.008.
37. MUSYOKA, S.M., MITTAL, H., MISHRA, S.B., NGILA, J.C., Effect of functionalization on the adsorption capacity of cellulose for the removal of methyl violet. International Journal of Biological Macromolecules, v. 65, p. 389-397, jun./jul, 2014. https://doi.org/10.1016/j.ijbiomac.2014.01.051.
38. PERUCHI, L.M., FOSTIER, A.H., RATH, S., Sorption of norfloxacin in soils: Analytical method, kinetics and Freundlich isotherms. Chemosphere, v. 119, p. 310-317, jun./jul, 2015. https://doi.org/10.1016/j.chemosphere.2014.06.008.
WEBER JR, W. J.; MORRIS, J. C. Kinetics of adsorption on carbon from solution. Journal of the sanitary engineering division, v. 89, n. 2, p. 31-59, 1963. https://doi.org/10.1061/JSEDAI.0000430.
39. GUPTA, S. S.; BHATTACHARYYA, K. G. Kinetics of adsorption of metal ions on inorganic materials: a review. Advances in Colloid and Interface Science, Amsterdam, v. 162, n. 1-2, p. 39-58, dez./jan, 2011. https://doi.org/10.1016/j.cis.2010.12.004.
40. AHMAD, R.; KUMAR, R. Adsorptive removal of congo red dye from aqueous solution using bael shell carbon. Applied Surface Science, Amsterdam, v. 257, n. 5, p. 1628-1633, nov./dez, 2010. https://doi.org/10.1016/j.apsusc.2010.08.111.
41. ALZAYDIEN, A. S.; MANASREH, W. Equilibrium, kinetic and thermodynamic studies on the adsorption of phenol onto activated phosphate rock. International Journal of Physical Sciences, Lagos, v. 4, n. 4, p. 172-181, 2009. Disponível em: https://academicjournals.org/journal/IJPS/article-full-text-pdf/B3C1A9F18737.
42. AHMED, M. J.; THEYDAN, S. K. Adsorption of cephalexin onto activated carbons from Albizia lebbeck seed pods by microwave-induced KOH and K2CO3 activations. Chemical Engineering Journal, Amsterdam, v. 211–212, n. 1, p. 200–207, 2012. https://doi.org/10.1016/j.cej.2012.09.089.
43. AHMED, M. J.; THEYDAN, S. K. Fluoroquinolones antibiotics adsorption onto microporous activated carbon from lignocellulosic biomass by microwave pyrolysis. Journal of the Taiwan Institute of Chemical Engineers, Taipei, v. 45, n. 1, p. 219–226, 2014. https://doi.org/10.1016/j.jtice.2013.05.014.
44. ARAUJO, A. L. P., SILVA, M. C. C., GIMENES, M. L., & BARROS, M. A. S. D.

Estudo termodinâmico da adsorção de zinco em argila bentonita bofe calcinada. Scientia plena, v. 5, n. 12, 2009. Disponível em: https://www.scientiaplena.org.br/sp/article/view/680.

45. LI, P., SU, Y.-J., WANG, Y., LIU, B., AND SUN, L.-M., Bioadsorption of methyl violet from aqueous solution onto Pu-erh tea powder. Journal of Hazardous Materials, 2010. 179(1–3): p. 43-48. https://doi.org/10.1016/j.jhazmat.2010.02.054.
AHMAD, R.; KUMAR, R. Adsorptive removal of congo red dye from aqueous solution using bael shell carbon. Applied Surface Science, Amsterdam, v. 257, n. 5, p. 1628-1633, nov./dez, 2010. https://doi.org/10.1016/j.apsusc.2010.08.111.
46. GERÇEL, Ö., ÖZCAN, A., ÖZCAN, A. S., & GERCEL, H. F. Preparation of activated carbon from a renewable bio-plant of Euphorbia rigida by H2SO4 activation and its adsorption behavior in aqueous solutions. Applied surface science, v. 253, n. 11, p. 4843-4852, 2007. https://doi.org/10.1016/j.apsusc.2010.08.111.

Research Highlights

- Encapsulating material from guava seed.
- High capacity to incorporate the methylene blue dye.
- Pseudo-second-order model better described the adsorption kinetics.